Benzothiazole Carboxylate Diester Bifunctional Chelators for ^{64}Cu PET imaging in Alzheimer's Disease

Yujue Wang, [†] Truc T. Huynh,[‡,#] Nilantha Bandara, [‡] Hong-Jun Cho,[†] Buck E. Rogers, [‡] and Liviu M. Mirica*[,†,§]

[†] Department of Chemistry, University of Illinois at Urbana-Champaign, 600 S. Mathews Avenue, Urbana, Illinois 61801, United States

[‡] Department of Radiation Oncology, Washington University School of Medicine, St. Louis, Missouri 63108, United States

Department of Chemistry, Washington University, St. Louis, Missouri 63130, United States

§Hope Center for Neurological Disorders, Washington University School of Medicine, St. Louis, MO 63110, United States

ABSTRACT

Herein we report a new series of bifunctional chelators (BFCs) with high affinity for amyloid β aggregates, strong binding affinity towards Cu(II), and favorable lipophilicity for potential blood-brain barrier (BBB) penetration. The alkyl carboxylate ester pendant arms enable high binding affinity towards Cu(II). The BFCs form stable ^{64}Cu-radiolabeled complexes and exhibit favorable partition coefficient (log D) values of 0.75-0.95. Among the five compounds tested, the **^{64}Cu-YW-1** and **^{64}Cu-YW-13** complexes exhibit significant staining of amyloid plaques in *ex vivo* autoradiography studies.

KEYWORDS

Alzheimer's disease, Amyloid beta plaques, ^{64}Cu positron emission tomography, lipophilicity

INTRODUCTION

According to the Alzheimer's Association, Alzheimer's disease (AD) is the 6th leading cause of death in the United States, and most common cause of dementia worldwide.[1] AD is a neurodegenerative disease, as the disease progresses, symptoms include memory loss, synaptic dysfunction, and decline in learning and thinking abilities.[2-4] As the disease progresses, amyloid plaques formed by abnormal aggregation of amyloid β (Aβ) gradually build up in brains of AD patients, causing brain damage and neuron death. Aβ peptides are derived from the amyloid precursor protein (APP), and sequential cleavages of APP by β- and γ-secretases generates Aβ monomers with 39 to 43 amino acid residues in length. The two major isoforms of Aβ peptide are 40 and 42 amino acids long, named $A\beta_{40}$ and $A\beta_{42}$, respectively.[5-9]

AD is currently incurable, and definitive diagnosis relies heavily on post-modern examination of brains of patients.[10-13] As researchers move to target early-stage of AD, determining the presence of amyloid deposits to confirm diagnosis becomes more and more important. Molecular imaging techniques, such as positron emission tomography (PET), have enabled non-invasive assessment of Aβ burden in brains of patients.[14, 15] PET imaging utilizes radiotracers containing positron-emitting radionuclides, such as ^{11}C ($t_{1/2}$= 20.4 min) and ^{18}F ($t_{1/2}$= 109.7 min), have been extensively studied in the last three decades. ^{11}C radiolabeled Pittsburgh Compound-B (^{11}C-PiB) is widely

used for imaging fibrillar amyloid species by PET scanning.[16, 17] Three ^{18}F-labelled Aβ tracers, the benzothiazole derivative ^{18}F-Flutemetamol (Vizamyl), the stilbene derivatives ^{18}F-Florbetaben (Neuraceq) and ^{18}F-Florbetapir (Amyvid) have been approved by the US Food and Drug Administration (FDA) for estimating Aβ plaque burdens in patients with cognitive impairment.[18-22]

However, in clinical usage, both ^{11}C and ^{18}F radiotracers suffer from the relatively short half-lives. In addition, these radioisotopes are covalently installed into the target molecules, requiring special synthetic approaches and equipment.[23] Therefore, long-lived radiometals, notably copper-64 ($t_{1/2}$ = 12.7 h, β^+ = 17.8%; β^- = 38.4%), have gained considerable interest in PET imaging.[24] Compared with ^{11}C and ^{18}F, the long half-life of ^{64}Cu allows for accumulation in the targeted region and broader clinical applications, especially for use in areas without access to on-site cyclotrons.[25-27] Moreover, ^{64}Cu could be easily incorporated into target bio-active agents via rapid chelation. The common oxidation state of ^{64}Cu in aqueous solution is ^{64}Cu(II), and its d^9 electronic configuration enables formation of many coordination forms, varying from four-coordinate to six-coordinate using metal chelators containing nitrogen donors, anionic oxygen, or sulfur donors.[24]

We have recently reported the development of bifunctional chelators (BFCs), which contain an Aβ-binding motif (2-phenylbenzothiazole derivative) and strong Cu(II)-chelating macrocyclic ligands, such as 1,4-dimethyl-1,4,7-triazacyclononane (TACN) and 2,11-diaza[3.3](2,6)pyridinophane (N4) macrocycles.[28-31] These BFCs exhibit high affinities for Aβ aggregates and Cu(II) ion, which could be used as ^{64}Cu amyloid PET imaging agents. The 2-phenylbenzothiazole derivative has shown appreciable Aβ-binding and fluorescent properties, therefore we continue to take advantage of this molecule as the amyloid binding motif and carry out the modification on the metal chelating fragment, by attaching two ester carboxylate pendant arms to the TACN backbone (Figure 1), in order to increase the lipophilicity of the bifunctional chelators (BFCs). Our purpose is to design diester-based ^{64}Cu PET imaging agents with favorable metal chelating ability and lipophilicity for *in vivo* amyloid PET imaging applications.

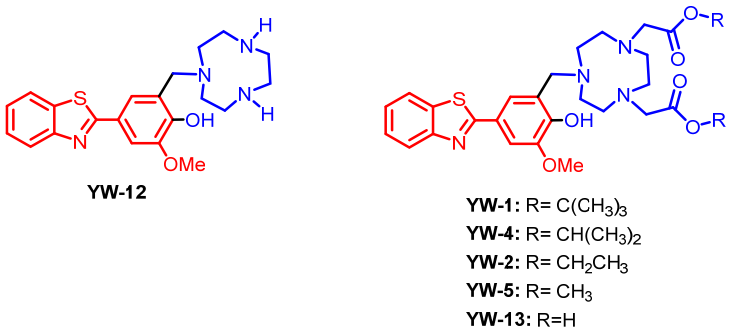

Figure 1. Structures of the ligands investigated herein. The metal-binding and Aβ-interacting fragments are shown in blue and red, respectively.

RESULTS AND DISCUSSION

Design and synthesis of BFCs. The bifunctional chelators (BFCs) discussed herein are created by linking the Aβ-binding fragment 2-(4-OH-phenyl)-benzothiazole and the metal-chelating TACN ligand via Mannich reaction (Scheme 1). The amyloid targeting motif was generated by the condensation of 2-aminothiophenol with vanillin, followed by oxidation with atmospheric oxygen (Scheme S1). To further enhance the metal chelation ability of BFCs, two pendant carboxylate arms were added to the TACN backbone.

Initially, the synthesis of final products was conducted by established procedures to generate the bi-substituted TACN ligands,[32] followed by Mannich reaction with 2-(4-OH-phenyl)-benzothiazole and paraformaldehyde (Scheme S2). However, due to the lack of fluorescence emission for these precursors, we failed to detect the unreacted TACN ligands by either TLC or HPLC, and therefore unable to separate the impurities from the products. Moreover, the heating condition could lead to decomposition of the ester products. Therefore, we developed a new pathway (Scheme 1) by synthesizing **YW-12** as the ligand precursor and then reacting **YW-12** with a series of alkyl-bromoacetates in presence of base, generating the final products **YW-1** to **YW-5** that contain tert-butyl, iso-propyl, ethyl, and methyl ester groups, respectively. Hydrolysis of **YW-1** in presence of concentrated hydrochloric acid generates **YW-13**.

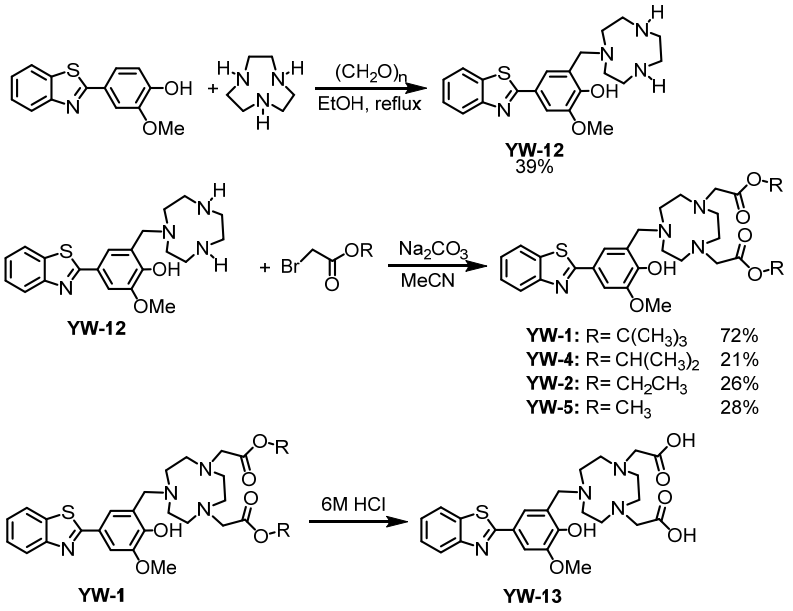

Scheme 1: Synthesis of BFCs

UV-Vis absorption spectra were acquired to determine the maximum absorbance wavelength (λ_{abs}) of the ligands and their Cu(II) complexes in PBS (pH=7.4) buffer (Figures S1, S2). Based on the UV-Vis absorbance spectra, excitation wavelengths (λ_{ex}) of 345-348 nm for BFCs and similar wavelengths for Cu(II) complexes were used to examine their fluorescent properties (Figures S3, S4). Due to the quenching effect by chelation with Cu(II), the fluorescence intensities of ester BFCs decrease by 3~4 folds, while that of **YW-13** decreases by 8 folds.

Interaction of YW-13 with Aβ_{42} fibrils. BFCs investigated herein contain fragments derived from benzothiazole and o-vanillin, which bind tightly to Aβ species.[33, 34] To further explore the amyloid affinity, we used Aβ_{42} fibrils and direct-binding fluorescent assays to measure the K_d values. As shown in Figure 2, **YW-13** shows nanomolar level binding towards Aβ_{42} fibrils with K_d = 121.0 ± 43.6 nM, indicating this BFC can bind tightly to Aβ_{42} species. We attempted to obtain K_d values for the ester BFCs, but the fluorescence intensities were low and barely changed with increasing concentrations of BFCs.

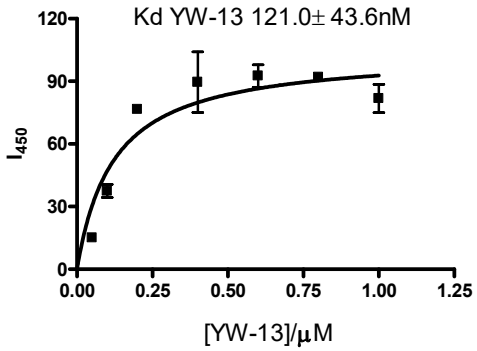

Figure 2. Direct binding constant measurements of **YW-13** with Aβ_{42} fibrils.

Fluorescence Imaging of Amyloid Plaques in 5xFAD Mouse Brain Sections. *Ex vivo* mouse brain section staining was performed to evaluate each BFC's affinity toward Aβ species. Brain sections were collected from 11-month-old 5xFAD transgenic mice, which overexpress mutant form of APP that can be cleaved by β- and γ-secretases to form Aβ peptides, and develop severe amyloid pathology found in AD.[35, 36] An appreciable amount of fluorescence staining was observed upon incubation of the brain sections for 30 min with 50 μM solutions of BFCs, especially for **YW-4** and **YW-5** (Figures 3, left panels). The specific staining of amyloid plaques was confirmed by staining with Congo Red, another amyloid-binding fluorescent dye (Figure 3, middle panels).[37, 38] The labeling ability of Cu(II) complexes was also probed using mouse brain sections of the same age. Compared to BFCs **YW-4** and **YW-5**, the colocalization of their Cu(II) complexes signal with Congo Red signal is improved, as indicated by Pearson's coefficients. The other BFCs and their Cu(II) complexes also show moderate staining of amyloid aggregates (Figures S5, S6). Overall, these *ex vivo* amyloid binding studies suggest that these BFCs could be bind to Aβ species (see below).

Ligand	Conc. (μM)	Ligand to Congo Red ratio
YW-4	50	25:1
Cu-YW-4	50	25:1
YW-5	50	25:1
Cu-YW-5	50	25:1

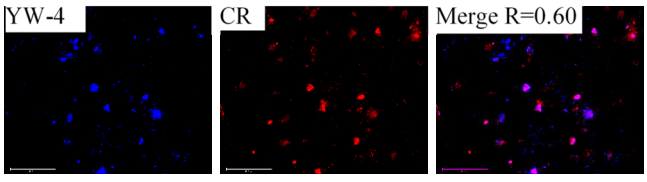

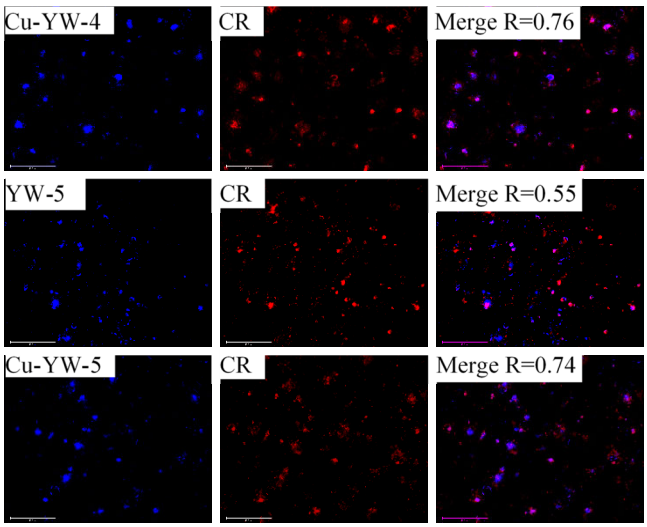

Figure 3. Fluorescence microscopy images of 5xFAD brain sections incubated with compound **YW-4, YW-5,** and their Cu(II) complexes (left panels), Congo Red (middle panels), and merged images (right panels). Magnification: 20x. Scale bar: 125μm.

The amyloid binding affinity of the BFCs was further investigated with AF594-conjugated HJ3.4 antibody (AF594-HJ3.4) that binds to a wide range of Aβ species.[31, 39-43] Using 6-month-old 5xFAD mouse brain sections, intense signal of fluorescence staining was observed with treatment of 50 μM BFCs or corresponding Cu(II) complexes solutions for 1 h. With less bulky substituents (from tert-butyl group to methyl group and hydrogen atom), there is an improvement of the colocalization between BFCs' signal and antibody signal, as indicated by the calculated Pearson's coefficients (Figure 4). The specific staining of **Cu-YW-13** is further examined with the 40x lens of the fluorescence microscope (Figure S7), and it exhibits strong colocalization with the antibody stained regions.

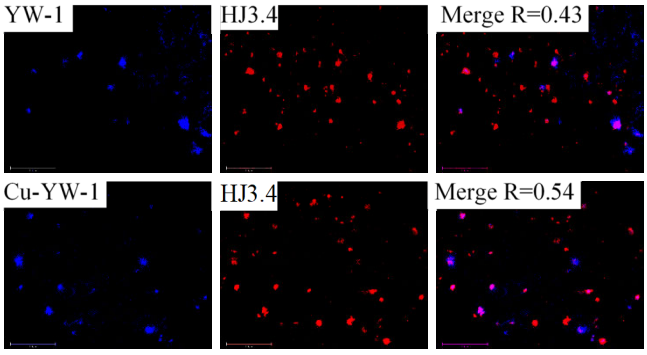

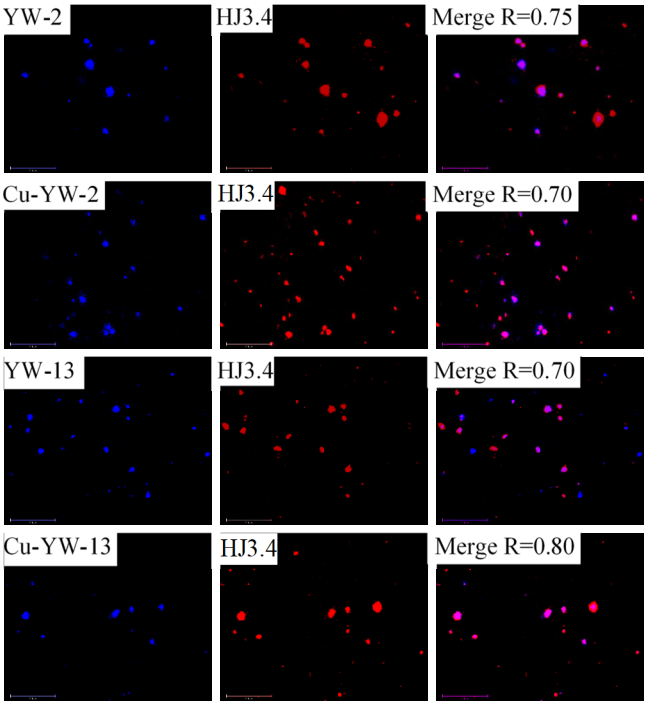

Figure 4. Fluorescence microscopy images of 5xFAD brain sections incubated with compound **YW-1, YW-2, YW-13** and their Cu(II) complexes (left panels), AF594-HJ3.4 antibody (middle panels), and merged images (right panels). Concentrations used: [BFC] = [Cu^{2+}] = 50 μM, [HJ3.4] = 1 μg/ml. Magnification: 20x. Scale bar: 125μm.

Stability Constants with Metal Ions by pH-Spectrophotometric Titration. Since all ligands contain several acidic and basic functional groups, their acidity constants (pKa) were determined by UV-Vis spectrophotometric titrations. In order to further investigate the metal chelation ability and to quantify it, we performed spectrophotometric titrations of ligands in presence of Cu(II) ion.

For **YW-1**, UV-Vis titrations from pH 3.0 to 11.0 reveal several changes in the spectra, such as the disappearance of the band at 325 nm and the in-crease of the band at 351 nm with an isosbestic point at 340 nm (Figure 5). The best fit to the data was obtained with four pKa values: 3.30(6), 5.75(5), 8.16(5) and 11.77(3) (Table 1). On the basis of previously reported acidity constants for phenols and amines,[34, 44] we assigned the three lower pKa values to the deprotonation of the amine groups on TACN backbone, and the highest pKa value to the phenol deprotonation in ligand. The other ester containing ligands in the series show similar values to those obtained for **YW-1**, as shown in Table 1.

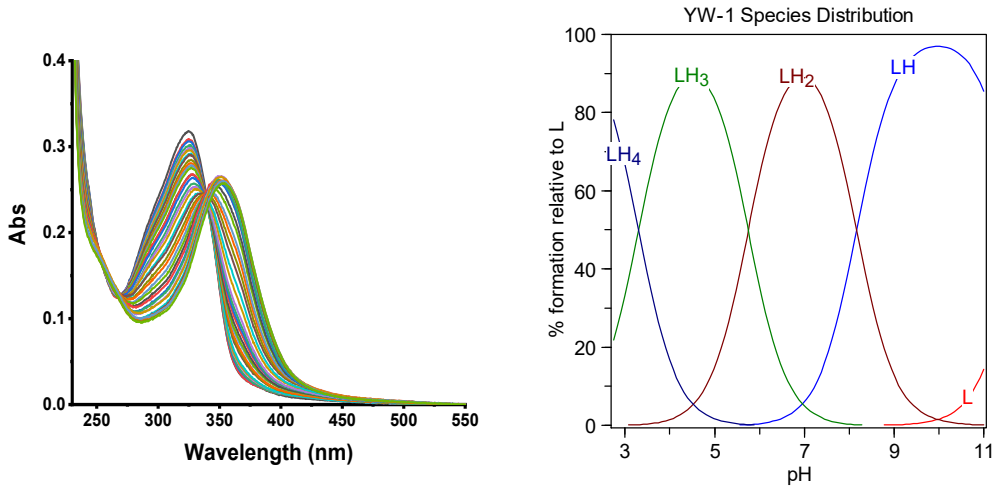

Figure 5. Variable pH (pH 3−11) UV-Vis spectra of **YW-1** ([L] = 20 μM, 25 °C, I = 0.1 M NaCl) and species distribution plot.

Similar spectrophotometric titrations were performed to determine the stability constants and solution speciation of Cu(II) with BFCs. The pKa values of the ligands and the deprotonation of metal-bound water molecules were included in the calculations. The stoichiometry of the Cu(II)-BFC complexes in solution was determined by Job's plot analysis. Plot of **Cu-YW-1** shows a break around 0.7 Cu mole fraction, and for other ester BFCs there are no clear breaks in the plots (Figures S16-S19), while for **Cu-YW-13** a break at ~0.5 Cu mole fraction suggests the formation of a 1:1 complex (Figure S20). The calculated stability constants show that **YW-1** has larger binding constants (logK) with Cu(II) than **YW-2, YW-4,** and **YW-5** (Table 2). In addition, **YW-13**, which contains two carboxylic groups instead of ester groups, exhibits the highest binding constant (logK) among all compounds, which is 2~3 orders of magnitude larger than those of ester BFCs.

The species distribution plot of **Cu-YW-1** was obtained based on the calculated stability constants (Figure 6), and the concentration of free Cu(II) with **YW-1** is negligible above pH 4, as shown in the plot. The concentrations of free Cu(II) (pM =−log[$M_{unchelated}$]) at a specific pH value and total ion concentration can be calculated from the solution speciation diagrams, and the calculated pCu values for **YW-1** and **YW-13** are 11.3 and 12.4 at pH 7.4, respectively, comparable to the value of 10.7 at pH 7.4 for the strong chelating agent DTPA (diethylenetriaminepentaacetic acid), indicating that our BFCs chelate strongly with Cu(II) ion.[34, 45, 46]

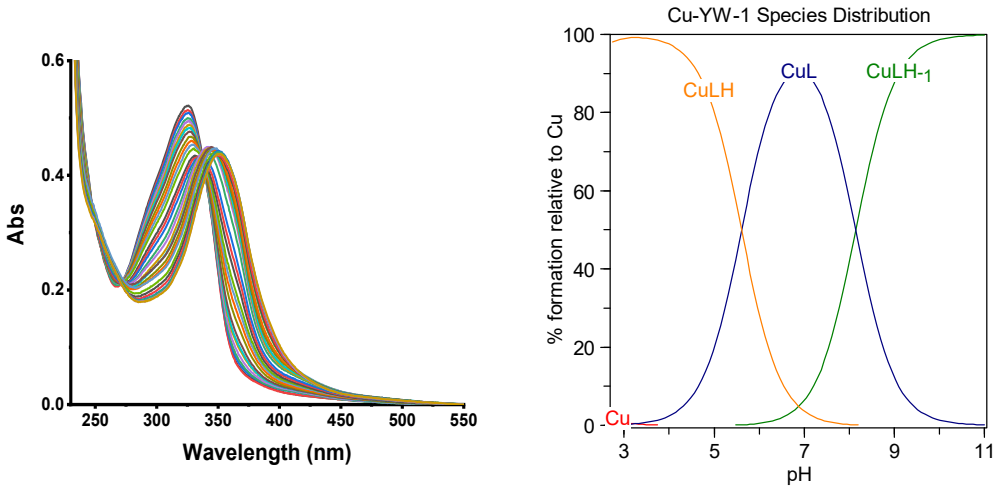

Figure 6. Variable pH (pH 3−11) UV-Vis spectra of **YW-1** and Cu(II) system ([L] = [Cu^{2+}] =20 μM, 25 °C, I = 0.1 M NaCl) and species distribution plot.

Table 1. Acidity constants (pK_a's) of **YW-1** to **YW-13** determined by spectrophotometric titrations (errors are for the last digit).

Reaction	YW-1	YW-4	YW-2	YW-5	YW-13
$[H_4L]^{3+} = [H_3L]^{2+} + H^+$ (pK_{a1})	3.30(6)	5.09(2)	4.78(3)	4.21(5)	3.83(5)
$[H_3L]^{2+} = [H_2L]^{+} + H^+$ (pK_{a2})	5.75(5)	6.48(1)	7.41(2)	6.90(2)	6.44(3)
$[H_2L]^{+} = [HL] + H^+$ (pK_{a3})	8.16(5)	8.27(1)	9.42(2)	12.82(1)	7.92(1)
$[HL] = [L]^{-} + H^+$ (pK_{a4})	11.77(3)	11.98(1)	11.36(1)	11.30(4)	11.84(1)

Table 2. Stability constants (logK) of the Cu(II) Complexes of **YW-1** to **YW-13**.

Reaction	YW-1	YW-4	YW-2	YW-5	YW-13
$M^{2+} + HL = [MHL]^{2+}$	5.61(13)	6.62(3)	6.89(9)	6.01(2)	3.89(3)
$M^{2+} + L^{-1} = [ML]^{+}$	23.41(9)	23.27(2)	22.79(7)	22.36(1)	25.56(6)
$[ML(H_2O)]^{+} = [ML(OH)] + H^+$	15.27(9)	14.98(2)	15.36(8)	13.79(2)	17.70(7)

Table 3. Calculated pM ($-\log[M]_{free}$; M = Cu^{2+}) values for a solution containing a 1:1 Metal/Ligand Mixture ($[M^{2+}]_{tot} = [Ligand]_{tot}$ = 50 μM)

	YW1	YW4	YW2	YW5	YW13	DTPA[a]
pH 6.6	10.5	10.3	9.6	9.4	11.5	9.7
pH 7.4	11.3	11.1	10.6	10.3	12.4	10.7

[a]Diethylenetriaminepentaacetic acid (DTPA).[45]

EPR spectra of copper complexes. To further characterize the copper complexes of ligands, their X-band EPR spectra were recorded in frozen glasses at 77 K. The copper complexes were prepared right before the EPR experiment by reacting ligand with 0.8 equivalent of $Cu(ClO_4)_2 \cdot 6H_2O$. The EPR spectrum of the **Cu-YW-1** in a 1:3 (v:v) MeCN:PrCN glass solution reveals a pseudoaxial EPR pattern with three different g values: g_x=2.258, g_y=2.060 and g_z=2.045, A_x(Cu)=159.24G (Figure 7). The EPR spectra of **Cu-YW-4** and **Cu-YW-5** were also obtained in the same way and exhibit a similar EPR pattern as **Cu-YW-1**'s with g_z = 2.255, A_z (Cu)=165 G, g_y = 2.055, g_x = 2.048, and g_z = 2.262, A_z (Cu) = 165 G, g_y = 2.041, g_x = 2.067, respectively (Figures S21, S22).

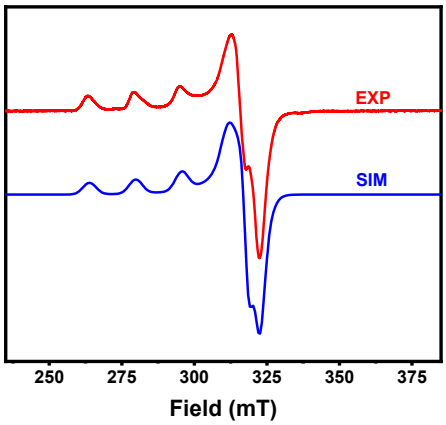

Figure 7. Experimental and simulated EPR spectra of the **Cu-YW-1** complex in 1:3 MeCN:PrCN glass at 77 K. The following parameters were used for the simulation: g_z=2.258, g_y=2.060, and g_x=2.045, A_z (Cu)=159 G.

In general, the R parameter [$R = (g_y - g_z)/(g_x - g_y)$ with $g_x > g_y > g_z$] can be indicative of the predominance of the d_z^2 or $d_{x^2-y^2}$ orbital in the ground state of the unpaired electron of the Cu^{2+} ion. When R > 1, the greater contribution to the ground state arises from the d_z^2 orbital, while when R < 1, the greater contribution to the ground state comes from the $d_{x^2-y^2}$ orbital. The R value of 0.076 determined for **Cu-YW-1** is indicative of a predominantly $d_{x^2-y^2}$ ground state, which is characteristic for Cu(II) complexes with slightly rhombic symmetry and elongation of the axial bonds. **Cu-YW-4** has a similar symmetry with an R value of 0.035.[47-49]

Radiolabeling and *Log D* value determination. The radiolabeling of compounds **YW-1** to **YW-13** was performed using $^{64}CuCl_2$ and employing the conditions described in the experimental

section.[50] Quality control assays were conducted using HPLC and/or TLC. All radiochemical yields were >95% within minutes at 45 °C, with specific activities of 100 Ci/mmol or greater. Therefore, all radiolabeled complexes were used directly without further purification.

For compounds to be used in neuroimaging applications, one critical factor is the penetration of blood brain barrier (BBB). Although the Lipinski's rules could offer insights for designing molecules with favorable lipophilicity, it is necessary to obtain experimental results for evaluation of BBB permeability.[51] To determine the hydrophobicity of the radiolabeled compounds, the octanol/water partition coefficient values *log D* were determined for the ^{64}Cu complexes of **YW-1** to **YW-13** (Table 3). Gratifyingly, the obtained *log D* values for the ^{64}Cu-radiolabeled complexes **YW-1** to **YW-5** are in the range of 0.72 - 0.95, which suggests their potential ability to cross the BBB. By comparison, the ^{64}Cu complex of **YW-13**, which does not contain ester group on the acetate branch, exhibits a negative *log D* values of −0.68±0.10 and thus is not expected to cross the BBB. The radio-HPLC profiles suggested **YW-13** chelate tightly with ^{64}Cu, while **^{64}Cu-YW-2** could undergo decomposition in the aqueous media, due to the potential hydrolysis of the ester groups (Figure S24).

Table 4. Molecular weights (MWs) of ligands **YW-1** to **YW-13**, measured *log D* values for the corresponding ^{64}Cu-radiolabeled complexes.

Ligand	MWs of ligands (g·mol^{-1})	*log D (^{64}Cu complexes)*
YW-1	626.8	0.95 ± 0.07
YW-4	598.3	0.91 ± 0.07
YW-2	570.7	0.90 ± 0.03
YW-5	542.7	0.72 ± 0.02
YW-13	514.6	-0.68 ± 0.10

Autoradiography studies. *Ex vivo* autoradiography studies using brain sections of 11-month-old 5xFAD and aged-matched WT mice were conducted to determine the specific binding of the ^{64}Cu-labeled BFCs to the amyloid plaques. The brain sections were stained, washed, and imaged as described in the experimental section.[50] Unfortunately, **^{64}Cu-YW-1** exhibits very low radioactivity intensity when staining the 5xFAD mouse brain sections (Figure 8, left column). Upon treatment with **^{64}Cu-YW-13** (Figure 8, right column), we observed an increased autoradiography intensity and **^{64}Cu-YW-13** exhibits a 2.26 intensity ratio of 5xFAD to WT staining (Figure 9). The specific

binding to amyloid plaques of the radiolabeled BFCs was further confirmed by blocking the brain sections with the non-radioactive blocking agent (**B_1**) (Figure S25).

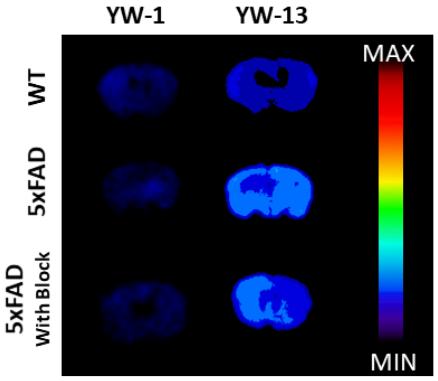

Figure 8. Autoradiography images of brain sections of WT and 5xFAD mice, in the absence and presence with a known Aβ specific blocking agent.

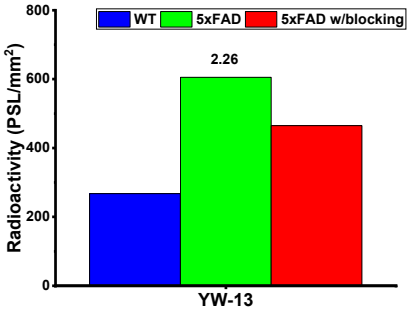

Figure 9. Average radioactivity of the brain sections in the autoradiography images. The numbers in the bar graph are the intensity ratios of 5xFAD to WT in each group.

CONCLUSIONS

To summarize, we have designed and synthesized five BFCs **YW-1** to **YW-13** containing a 2-(4-hydroxyphenyl)benzothiazole fragment as the amyloid targeting motif and triazacyclononane-based metal chelators. Modification of the synthetic pathway allows for the generation of a series of BFCs in a direct approach. The evaluation of the Aβ-binding affinity for these BFCs and their ^{64}Cu complexes was probed by *ex vivo* AD mouse brain section fluorescence imaging and autoradiography studies. These results show that the Cu(II) complexes of the carboxylate acid BFC **YW-13** bind more selectively to the amyloid plaques than the Cu(II) complexes of the carboxylic ester BFCs **YW-1** to **YW-5**. The ^{64}Cu-radiolabeled carboxylate ester BFCs exhibit moderate *log*

D values around 0.9, suggesting they should be BBB permeable. Unfortunately, the ^{64}Cu complex of **YW-13**, which has favorable amyloid binding affinity and metal chelating ability, exhibits a negative *log D* value.

Overall, the resulting BFCs could be readily radiolabeled with ^{64}Cu for PET imaging purposes. More efforts need to be devoted to improve the lipophilicity of such BFCs for *in vivo* applications.

ASSOCIATED CONTENT

Supporting Information. Spectrophotometric titrations, Job's plots, UV−Vis and fluorescence spectra, HPLC chromatograms of radiolabeling assays.

AUTHOR INFORMATION

Corresponding Author

* mirica@illinois.edu

Notes

The authors declare no competing financial interest.

ORCID

Liviu Mirica: 0000-0003-0584-9508

Yujue Wang: 0000-0002-5644-5952

ACKNOWLEDGMENTS

This work was supported by research funding from the NIH (R01GM114588 to L.M.M.). We thank the small animal imaging facilities at Washington University School of Medicine for excellent technical assistance and the Isotope Production Group at Washington University for the production of ^{64}Cu.

REFERENCES

1. 2020 Alzheimer's disease facts and figures. *Alzheimer's & Dementia* **2020,** *16*, 391-460.
2. Duyckaerts, C.; Delatour, B.; Potier, M. C., Classification and basic pathology of Alzheimer disease. *Acta Neuropathol* **2009,** *118*, 5-36.
3. Jack, C. R., Jr.; Bennett, D. A.; Blennow, K.; Carrillo, M. C.; Dunn, B.; Haeberlein, S. B.; Holtzman, D. M.; Jagust, W.; Jessen, F.; Karlawish, J.; Liu, E.; Molinuevo, J. L.; Montine, T.; Phelps, C.; Rankin, K. P.; Rowe, C. C.; Scheltens, P.; Siemers, E.; Snyder, H. M.; Sperling, R.; Contributors, NIA-AA Research Framework: Toward a biological definition of Alzheimer's disease. *Alzheimer's & Dementia* **2018,** *14*, 535-562.
4. Mayeux, R.; Stern, Y., Epidemiology of Alzheimer disease. *Cold Spring Harbor Persp. Med.* **2012,** *2*.
5. Kasim, J. K.; Kavianinia, I.; Harris, P. W. R.; Brimble, M. A., Three Decades of Amyloid Beta Synthesis: Challenges and Advances. *Front Chem* **2019,** *7*, 472.
6. Thinakaran, G.; Koo, E. H., Amyloid precursor protein trafficking, processing, and function. *J. Biol. Chem.* **2008,** *283*, 29615-9.
7. Chen, G. F.; Xu, T. H.; Yan, Y.; Zhou, Y. R.; Jiang, Y.; Melcher, K.; Xu, H. E., Amyloid beta: structure, biology and structure-based therapeutic development. *Acta Pharmacol. Sin.* **2017,** *38*, 1205-1235.
8. Zhang, Y. W.; Thompson, R.; Zhang, H.; Xu, H., APP processing in Alzheimer's disease. *Molecular brain* **2011,** *4*, 3.
9. Pauwels, K.; Williams, T. L.; Morris, K. L.; Jonckheere, W.; Vandersteen, A.; Kelly, G.; Schymkowitz, J.; Rousseau, F.; Pastore, A.; Serpell, L. C.; Broersen, K., Structural Basis for Increased Toxicity of Pathological Aβ42:Aβ40 Ratios in Alzheimer Disease. *J. Biol. Chem.* **2012,** *287*, 5650-5660.
10. Cummings, J. L.; Morstorf, T.; Zhong, K., Alzheimer's disease drug-development pipeline: few candidates, frequent failures. *Alzheimers Res. Ther.* **2014,** *6*.
11. Cummings, J.; Lee, G.; Ritter, A.; Sabbagh, M.; Zhong, K., Alzheimer's disease drug development pipeline: 2020. *Alzheimer's & Dement.* **2020,** *6*, e12050.
12. Hardy, J.; Allsop, D., Amyloid deposition as the central event in the aetiology of Alzheimer's disease. *Trends Pharmacol. Sci.* **1991,** *12*, 383-8.
13. Vallet, P. G.; Guntern, R.; Hof, P. R.; Golaz, J.; Delacourte, A.; Robakis, N. K.; Bouras, C., A comparative study of histological and immunohistochemical methods for neurofibrillary tangles and senile plaques in Alzheimer's disease. *Acta Neuropathol* **1992,** *83*, 170-8.
14. Ametamey, S. M.; Honer, M.; Schubiger, P. A., Molecular imaging with PET. *Chem. Rev.* **2008,** *108*, 1501-16.
15. Czernin, J.; Phelps, M. E., Positron emission tomography scanning: current and future applications. *Annu. Rev. Med.* **2002,** *53*, 89-112.
16. Klunk, W. E.; Engler, H.; Nordberg, A.; Wang, Y.; Blomqvist, G.; Holt, D. P.; Bergström, M.; Savitcheva, I.; Huang, G.-F.; Estrada, S.; Ausén, B.; Debnath, M. L.; Barletta, J.; Price,

J. C.; Sandell, J.; Lopresti, B. J.; Wall, A.; Koivisto, P.; Antoni, G.; Mathis, C. A.; Långström, B., Imaging Brain Amyloid in Alzheimer's Disease with Pittsburgh Compound-B. *Ann. Neurol.* **2004,** *55*, 306-319.

17. Frederiksen, K. S.; Hasselbalch, S. G.; Hejl, A. M.; Law, I.; Hojgaard, L.; Waldemar, G., Added Diagnostic Value of (11)C-PiB-PET in Memory Clinic Patients with Uncertain Diagnosis. *Dement. Geriat. Cognit. Dis.* **2012,** *2*, 610-21.
18. Serdons, K.; Terwinghe, C.; Vermaelen, P.; Van Laere, K.; Kung, H.; Mortelmans, L.; Bormans, G.; Verbruggen, A., Synthesis and evaluation of ^{18}F-labeled 2-phenylbenzothiazoles as positron emission tomography imaging agents for amyloid plaques in Alzheimer's disease. *J. Med. Chem.* **2009,** *52*, 1428-1437.
19. Choi, S. R.; Golding, G.; Zhuang, Z.; Zhang, W.; Lim, N.; Hefti, F.; Benedum, T. E.; Kilbourn, M. R.; Skovronsky, D.; Kung, H. F., Preclinical Properties of 18F-AV-45: A PET Agent for Aβ Plaques in the Brain. *J. Nucl. Med.* **2009,** *50*, 1887-1894.
20. Uzuegbunam, B. C.; Librizzi, D.; Yousefi, B. H., PET Radiopharmaceuticals for Alzheimer's Disease and Parkinson's Disease Diagnosis, the Current and Future Landscape. *Molecules* **2020,** *25*.
21. Kung, H. F.; Choi, S. R.; Qu, W.; Zhang, W.; Skovronsky, D., ^{18}F Stilbenes and Styrylpyridines for PET Imaging of Aβ Plaques in Alzheimer's Disease: A Miniperspective. *J. Med. Chem.* **2010,** *53*, 933-941.
22. Herholz, K.; Ebmeier, K., Clinical amyloid imaging in Alzheimer's disease. *Lancet Neurol.* **2011,** *10*, 667-70.
23. Conti, M.; Eriksson, L., Physics of pure and non-pure positron emitters for PET: a review and a discussion. *EJNMMI physics* **2016,** *3*, 8.
24. Shokeen, M.; Anderson, C. J., Molecular Imaging of Cancer with Copper-64 Radiopharmaceuticals and Positron Emission Tomography (PET). *Acc. Chem. Res.* **2009,** *42*, 832-841.
25. Maheshwari, V.; Dearling, J. L. J.; Treves, S. T.; Packard, A. B., Measurement of the rate of copper(II) exchange for 64Cu complexes of bifunctional chelators. *Inorg. Chim. Acta* **2012,** *393*, 318-323.
26. Sedgwick, A. C.; Brewster, J. T.; Harvey, P.; Iovan, D. A.; Smith, G.; He, X.-P.; Tian, H.; Sessler, J. L.; James, T. D., Metal-based Imaging Agents: Progress towards Interrogating Neurodegenerative Disease. *Chem. Soc. Rev.* **2020,** *49*, 2886-2915.
27. Wadas, T. J.; Wong, E. H.; Weisman, G. R.; Anderson, C. J., Copper chelation chemistry and its role in copper radiopharmaceuticals. *Curr. Pharm. Des.* **2007,** *13*, 3-16.
28. Sharma, A. K.; Schultz, J. W.; Prior, J. T.; Rath, N. P.; Mirica, L. M., Coordination Chemistry of Bifunctional Chemical Agents Designed for Applications in Cu-64 PET Imaging for Alzheimer's Disease. *Inorg. Chem.* **2017,** *56*, 13801-13814.
29. Huang, Y.; Cho, H.-J.; Bandara, N.; Sun, L.; Tran, D.; Rogers, B. E.; Mirica, L. M., Metal-chelating benzothiazole multifunctional compounds for the modulation and 64Cu PET imaging of Aβ aggregation. *Chem. Sci.* **2020,** *11*, 7789-7799.

30. Cho, H. J.; Huynh, T. T.; Rogers, B. E.; Mirica, L. M., Design of a multivalent bifunctional chelator for diagnostic (64)Cu PET imaging in Alzheimer's disease. *Proc. Natl. Acad. Sci. U. S. A.* **2020,** *117*, 30928-30933.
31. Cho, H. J.; Huynh, T. T.; Rogers, B. E.; Mirica, L. M., Design of a multivalent bifunctional chelator for diagnostic (64)Cu PET imaging in Alzheimer's disease. *Proc Natl Acad Sci U S A* **2020,** *117*, 30928-30933.
32. Chong, H.-S.; Sun, X.; Zhong, Y.; Bober, K.; Lewis, M. R.; Liu, D.; Ruthengael, V. C.; Sin, I.; Kang, C. S., Synthesis and Evaluation of an Enantiomerically Enriched Bifunctional Chelator for64Cu-Based Positron Emission Tomography (PET) Imaging. *Eur. J. Org. Chem.* **2014,** *2014*, 1305-1313.
33. Necula, M.; Kayed, R.; Milton, S.; Glabe, C. G., Small molecule inhibitors of aggregation indicate that amyloid β oligomerization and fibrillization pathways are independent and distinct. *J. Biol. Chem.* **2007,** *282*, 10311-10324.
34. Sharma, A. K.; Pavlova, S. T.; Kim, J.; Finkelstein, D.; Hawco, N. J.; Rath, N. P.; Kim, J.; Mirica, L. M., Bifunctional Compounds for Controlling Metal-mediated Aggregation of the $A\beta_{42}$ Peptide. *J. Am. Chem. Soc.* **2012,** *134*, 6625-6636.
35. Oakley, H.; Cole, S. L.; Logan, S.; Maus, E.; Shao, P.; Craft, J.; Guillozet-Bongaarts, A.; Ohno, M.; Disterhoft, J.; Van Eldik, L.; Berry, R.; Vassar, R., Intraneuronal β-amyloid aggregates, neurodegeneration, and neuron loss in transgenic mice with five familial Alzheimer's disease mutations: potential factors in amyloid plaque formation. *J. Neurosci.* **2006,** *26*, 10129-10140.
36. Drummond, E.; Wisniewski, T., Alzheimer's disease: experimental models and reality. *Acta Neuropathol* **2017,** *133*, 155-175.
37. Klunk, W. E.; Pettegrew, J. W.; Abraham, D. J., Quantitative evaluation of congo red binding to amyloid-like proteins with a beta-pleated sheet conformation. *J. Histochem. Cytochem.* **1989,** *37*, 1273-81.
38. Yakupova, E. I.; Bobyleva, L. G.; Vikhlyantsev, I. M.; Bobylev, A. G., Congo Red and amyloids: history and relationship. *Biosci. Rep.* **2019,** *39*.
39. Schwetye, K. E.; Cirrito, J. R.; Esparza, T. J.; Mac Donald, C. L.; Holtzman, D. M.; Brody, D. L., Traumatic Brain Injury Reduces Soluble Extracellular Amyloid-β in Mice: A Methodologically Novel Combined Microdialysis-Controlled Cortical Impact Study. *Neurobiol. Dis.* **2010,** *40*, 555-564.
40. Esparza, T. J.; Wildburger, N. C.; Jiang, H.; Gangolli, M.; Cairns, N. J.; Bateman, R. J.; Brody, D. L., Soluble Amyloid-beta Aggregates from Human Alzheimer's Disease Brains. *Sci. Rep.* **2016,** *6*, 38187.
41. Perrin, R. J.; Fagan, A. M.; Holtzman, D. M., Multimodal Techniques for Diagnosis and Prognosis of Alzheimer's Disease. *Nature* **2009,** *461*, 916-922.
42. Fagan, A. M.; Holtzman, D. M., Cerebrospinal fluid biomarkers of Alzheimer's disease. *Biomark Med* **2010,** *4*, 51-63.

43. Sun, L.; Sharma, A. K.; Han, B.-H.; Mirica, L. M., Amentoflavone: A Bifunctional Metal Chelator that Controls the Formation of Neurotoxic Soluble Aβ42 Oligomers. *ACS Chem. Neurosci.* **2020,** *11*, 2741-2752.
44. Bandara, N.; Sharma, A. K.; Krieger, S.; Schultz, J. W.; Han, B. H.; Rogers, B. E.; Mirica, L. M., Evaluation of ^{64}Cu-based Radiopharmaceuticals That Target Aβ Peptide Aggregates as Diagnostic Tools for Alzheimer's Disease. *J. Am. Chem. Soc.* **2017,** *139*, 12550-12558.
45. Storr, T.; Merkel, M.; Song-Zhao, G. X.; Scott, L. E.; Green, D. E.; Bowen, M. L.; Thompson, K. H.; Patrick, B. O.; Schugar, H. J.; Orvig, C., Synthesis, characterization, and metal coordinating ability of multifunctional carbohydrate-containing compounds for Alzheimer's therapy. *J. Am. Chem. Soc.* **2007,** *129*, 7453-7463.
46. Choudhary, N.; Jaraquemada-Pelaez, M. D.; Zarschler, K.; Wang, X. Z.; Radchenko, V.; Kubeil, M.; Stephan, H.; Orvig, C., Chelation in One Fell Swoop: Optimizing Ligands for Smaller Radiometal Ions. *Inorg. Chem.* **2020,** *59*, 5728-5741.
47. Esteves, C. V.; Lamosa, P.; Delgado, R.; Costa, J.; Désogère, P.; Rousselin, Y.; Goze, C.; Denat, F., Remarkable Inertness of Copper(II) Chelates of Cyclen-Based Macrobicycles with Two trans-N-Acetate Arms. *Inorg. Chem.* **2013,** *52*, 5138-5153.
48. Hathaway, B. J.; Billing, D. E., The electronic properties and stereochemistry of mono-nuclear complexes of the copper(II) ion. *Coord. Chem. Rev.* **1970,** *5*, 143-207.
49. Hathaway, B. J.; Tomlinson, A. A. G., Copper(II) ammonia complexes. *Coord. Chem. Rev.* **1970,** *5*, 1-43.
50. See Supporting Information.
51. Lipinski, C. A.; Lombardo, F.; Dominy, B. W.; Feeney, P. J., Experimental and computational approaches to estimate solubility and permeability in drug discovery and development settings. *Adv. Drug Delivery Rev.* **2001,** *46*, 3-26.